BEHAVIOR OF HORIZONTAL AND VERTICAL SV AT JMA SITES, JAPAN

By Mehedi Ahmed Ansary[1] and Fumio Yamazaki[2]

ABSTRACT: Characteristics of response spectra of free-field horizontal and vertical ground motion recorded by JMA-87 type accelerometers are examined. The database includes 2,166 response spectra of motions from 387 events recorded at 76 JMA sites (70% on hard soil or rock and 30% on medium to soft soil). Most of the ground motions are far-source records. Relative spectral velocities at 0, 2, and 5% critical damping for 22 periods in the range of engineering interest have been subjected to nonlinear regression procedures in terms of magnitude and hypocentral distance. The attenuation relations consider the effect of depth and the local site amplification. A numerical technique called iterative partial regression is used to apply Joyner and Boore's two-stage regression methodology while considering the effect of the recording site. Dependence of horizontal and vertical response spectra, and their ratio, on magnitude, site-to-source distance, and depth are investigated through the development of attenuation relationships for horizontal and vertical spectral ordinates. The horizontal-to-vertical (H/V) response spectral ratio is found to be strongly dependent on period. At short periods, the value of the H/V spectral ratio is 1.5, but with an increase in period from an intermediate to a longer range, the spectral ratio attains a value of 3. These characteristics of H/V spectral ratio are likely to be universal for far-source recordings. The frequency-dependent relative amplification of the sites are found to be distinctive from site to site, and it is found that stations with the same soil type classification show an apparent pattern. Because the local site characteristics are explicitly derived, the resulting predictive equations can be considered as site-specific response spectra for the 76 JMA stations examined here.

INTRODUCTION

In a previous study (Molas and Yamazaki 1995a), 2,166 recorded peak ground motion parameters of moderate-to-large earthquakes observed by 76 JMA-87 type digital accelerometers in Japan (Fig. 1) are examined.

There exist a few attenuation models which deal with Fourier amplitudes (Mamula et al. 1984; Trifunac and Lee 1989), $FS(T)$, and relative velocity spectral amplitudes (Joyner and Boore 1982; Bozorgnia and Niazi 1993; Lee 1993; Bozorgnia et al. 1995), $S_V(\zeta, T)$. Theoretically, for low damping values, Fourier amplitude can be represented by relative velocity spectral amplitude (Ohsaki 1994). The same form of attenuation models are used for both types of spectral amplitudes (Lee 1993). Although Trifunac and Lee's (1989) attenuation relation considers local soil type, local geologic conditions (depth of sediments), and directional dependence of amplification, these factors are still inadequate to take care of the local site amplification reliably. More recently, Bozorgnia and Niazi (1993) and Bozorgnia et al. (1995) estimated attenuation models for relative velocity spectral amplitudes for specific fault areas and particular soil types.

In this study, a new attenuation model proposed by Molas and Yamazaki (1995a) is used, where site amplification is taken care of by assigning a dummy variable at each JMA station. This is possible due to the recording of several earthquake events at each station. The purpose of this paper is to present a summary of our recent study on scaling of the relative spectral velocity (SV).

DATA

The acceleration time histories are recorded from August 1, 1988, to December 31, 1993, and consist mostly of far-source records. In this study, records with peak ground accelerations

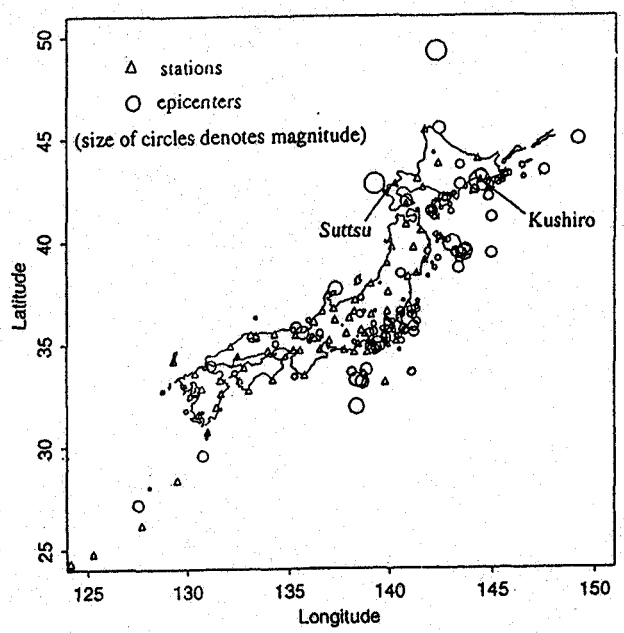

FIG. 1. Map of Locations of JMA Recording Stations and Earthquake Epicenters Used in This Study

TABLE 1. Summary of Data Used in This Study

Parameter (1)	Characteristic (2)
Number of events	387
Number of records	2,166
Number of recording stations	76
Date recorded	August 1, 1988–December 31, 1993
Instrument	JMA-87 type accelerometers
Recording institution	Japan Meteorological Agency (JMA)
Magnitude range	4.0–7.8 (JMA scale)
Minimum acceleration (larger of two horizontal components)	PGA ≥ 1.0 gal
Depth range	0.1–200 km
Structural periods analyzed	0.05, 0.06, 0.075, 0.10, 0.12, 0.15, 0.17, 0.20, 0.25, 0.30, 0.40, 0.50, 0.75, 1.0, 1.5, 2.0, 3.0, 4.0, 5.0, 7.5, 10.0, 15.0
Damping coefficient	0, 2, and 5% of critical

[1]Asst. Prof., Dept. of Civ. Engrg., Bangladesh Univ. of Engrg. and Technol., Dhaka-1000, Bangladesh.

[2]Assoc. Prof., Dept. of Civ. Engrg., Inst. of Indust. Sci., Univ. of Tokyo, 7-22-1, Roppongi, Tokyo-106, Japan.

Note. Discussion open until December 1, 1998. To extend the closing date one month, a written request must be filed with the ASCE Manager of Journals. The manuscript for this paper was submitted for review and possible publication on April 29, 1997. This paper is part of the ***Journal of Geotechnical and Geoenvironmental Engineering***, Vol. 124, No. 7, July, 1998. ©ASCE, ISSN 1090-0241/98/0007-0606–0616/$8.00 + $.50 per page. Paper No. 15662.

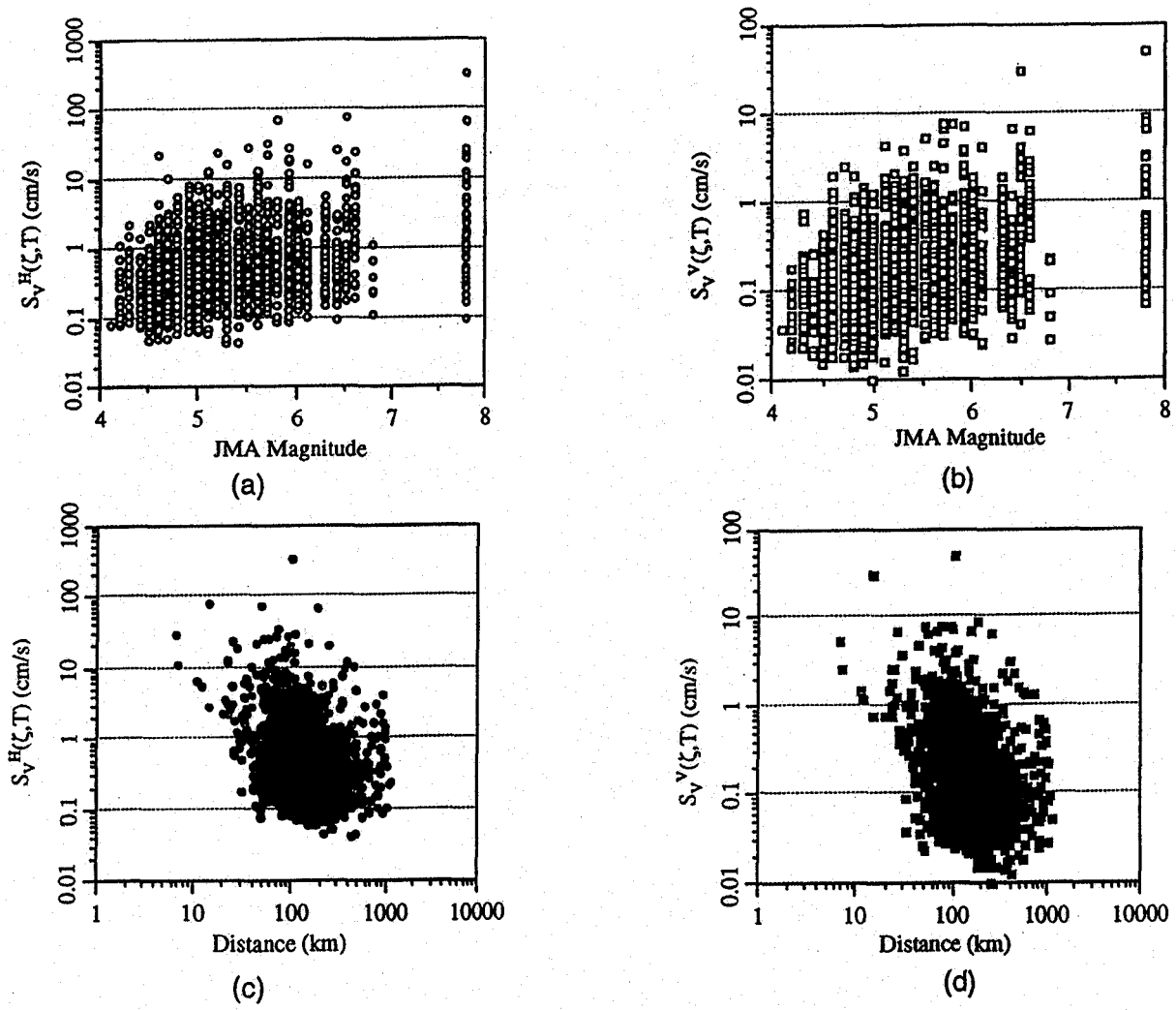

FIG. 2. Distribution of: (a) Magnitude and Horizontal Spectral Velocity; (b) Magnitude and Vertical Spectral Velocity; (c) Distance and Horizontal Spectral Velocity; and (d) Distance and Vertical Spectral Velocity of Records for 5% Damping and $T = 0.5$ s

TABLE 2. Regression Coefficients for Relative Velocity Response Spectrum $S_V^H(0.00, T)$ (in cm/s)

T (sec) (1)	b_0 (2)	b_1 (3)	b_2 (4)	b_3 (5)	b_4 (6)	σ_r (7)	σ_e (8)	σ (9)
0.05	−1.6029	0.3757	−0.00116	−1.00	0.00372	0.244	0.169	0.297
0.06	−1.3452	0.3853	−0.00144	−1.00	0.00425	0.253	0.183	0.312
0.075	−1.1337	0.4034	−0.00157	−1.00	0.00457	0.258	0.183	0.316
0.10	−0.8226	0.4152	−0.00171	−1.00	0.00468	0.256	0.198	0.324
0.12	−0.5758	0.4114	−0.00162	−1.00	0.00423	0.254	0.194	0.319
0.15	−0.5287	0.4485	−0.00161	−1.00	0.00378	0.250	0.190	0.314
0.17	−0.5362	0.4656	−0.00153	−1.00	0.00367	0.250	0.168	0.300
0.20	−0.4630	0.4730	−0.00140	−1.00	0.00330	0.257	0.150	0.298
0.25	−0.6014	0.5133	−0.00129	−1.00	0.00289	0.251	0.140	0.288
0.30	−0.6968	0.5429	−0.00119	−1.00	0.00277	0.248	0.134	0.282
0.40	−0.9519	0.6024	−0.00122	−1.00	0.00216	0.232	0.148	0.275
0.50	−1.1524	0.6403	−0.00111	−1.00	0.00170	0.224	0.131	0.260
0.75	−1.7692	0.7491	−0.00113	−1.00	0.00129	0.221	0.141	0.262
1.00	−2.1370	0.7992	−0.00105	−1.00	0.00093	0.226	0.120	0.256
1.50	−2.4156	0.8241	−0.00102	−1.00	0.00071	0.223	0.115	0.251
2.00	−2.4829	0.8171	−0.00102	−1.00	0.00100	0.231	0.111	0.256
3.00	−2.3751	0.7763	−0.00115	−1.00	0.00138	0.239	0.104	0.260
4.00	−2.2107	0.7333	−0.00113	−1.00	0.00164	0.236	0.100	0.257
5.00	−2.1033	0.7092	−0.00116	−1.00	0.00165	0.239	0.103	0.260
7.50	−1.9394	0.6715	−0.00111	−1.00	0.00162	0.243	0.103	0.264
10.00	−1.8836	0.6638	−0.00110	−1.00	0.00151	0.240	0.118	0.267
15.00	−1.6583	0.6170	−0.00101	−1.00	0.00165	0.235	0.105	0.257

Note: σ_r^2 = record-to-record component of variance (determined in second step); σ_e^2 = earthquake-to-earthquake component of variance (determined in third step); σ^2 = total variance $\cong \sigma_r^2 + \sigma_e^2$.

TABLE 3. Regression Coefficients for Relative Velocity Response Spectrum $S_V^V(0.00, T)$ (in cm/s)

T (sec) (1)	b_0 (2)	b_1 (3)	b_2 (4)	b_3 (5)	b_4 (6)	σ_r (7)	σ_e (8)	σ (9)
0.05	−1.7596	0.3883	−0.00124	−1.00	0.00399	0.246	0.158	0.293
0.06	−1.5137	0.3972	−0.00149	−1.00	0.00446	0.261	0.173	0.314
0.075	−1.2792	0.4167	−0.00170	−1.00	0.00472	0.260	0.188	0.321
0.10	−1.0194	0.4325	−0.00176	−1.00	0.00447	0.255	0.191	0.319
0.12	−0.9901	0.4531	−0.00168	−1.00	0.00428	0.246	0.182	0.306
0.15	−0.8935	0.4672	−0.00155	−1.00	0.00394	0.240	0.177	0.298
0.17	−0.9015	0.4771	−0.00150	−1.00	0.00369	0.243	0.161	0.292
0.20	−0.8936	0.4863	−0.00141	−1.00	0.00330	0.246	0.144	0.286
0.25	−1.0343	0.5233	−0.00130	−1.00	0.00288	0.232	0.145	0.274
0.30	−1.1289	0.5486	−0.00118	−1.00	0.00265	0.233	0.127	0.266
0.40	−1.5240	0.6256	−0.00115	−1.00	0.00194	0.224	0.147	0.268
0.50	−1.7746	0.6700	−0.00114	−1.00	0.00165	0.221	0.147	0.266
0.75	−2.3276	0.7675	−0.00099	−1.00	0.00082	0.219	0.140	0.259
1.00	−2.7368	0.8313	−0.00086	−1.00	0.00033	0.216	0.129	0.251
1.50	−2.9734	0.8480	−0.00086	−1.00	0.00043	0.203	0.126	0.239
2.00	−2.9989	0.8330	−0.00076	−1.00	0.00045	0.205	0.110	0.233
3.00	−2.8894	0.7944	−0.00093	−1.00	0.00081	0.206	0.112	0.234
4.00	−2.7064	0.7474	−0.00092	−1.00	0.00104	0.201	0.120	0.234
5.00	−2.5945	0.7219	−0.00096	−1.00	0.00123	0.207	0.118	0.238
7.50	−2.3270	0.6621	−0.00082	−1.00	0.00131	0.206	0.119	0.238
10.00	−2.1709	0.6317	−0.00070	−1.00	0.00128	0.204	0.123	0.239
15.00	−1.9104	0.5810	−0.00061	−1.00	0.00140	0.205	0.115	0.235

TABLE 4. Regression Coefficients for Relative Velocity Response Spectrum $S_V^H(0.02, T)$ (in cm/s)

T (sec) (1)	b_0 (2)	b_1 (3)	b_2 (4)	b_3 (5)	b_4 (6)	σ_r (7)	σ_e (8)	σ (9)
0.05	−1.8997	0.3792	−0.00182	−1.00	0.00424	0.268	0.179	0.322
0.06	−1.6373	0.3752	−0.00189	−1.00	0.00449	0.274	0.177	0.326
0.075	−1.3705	0.3832	−0.00199	−1.00	0.00461	0.278	0.192	0.338
0.10	−0.9802	0.3784	−0.00197	−1.00	0.00465	0.277	0.193	0.337
0.12	−0.7882	0.3843	−0.00192	−1.00	0.00445	0.273	0.192	0.334
0.15	−0.6324	0.4006	−0.00180	−1.00	0.00400	0.274	0.183	0.330
0.17	−0.6410	0.4211	−0.00172	−1.00	0.00381	0.273	0.161	0.317
0.20	−0.6077	0.4358	−0.00156	−1.00	0.00344	0.274	0.148	0.311
0.25	−0.7203	0.4780	−0.00149	−1.00	0.00313	0.263	0.142	0.299
0.30	−0.7862	0.5038	−0.00141	−1.00	0.00297	0.259	0.132	0.291
0.40	−0.9935	0.5571	−0.00139	−1.00	0.00252	0.246	0.132	0.279
0.50	−1.1358	0.5868	−0.00130	−1.00	0.00225	0.239	0.118	0.266
0.75	−1.5870	0.6712	−0.00123	−1.00	0.00180	0.232	0.120	0.261
1.00	−1.8828	0.7156	−0.00117	−1.00	0.00153	0.228	0.113	0.254
1.50	−2.1044	0.7403	−0.00116	−1.00	0.00143	0.225	0.107	0.249
2.00	−2.1734	0.7407	−0.00117	−1.00	0.00153	0.228	0.105	0.250
3.00	−2.1650	0.7269	−0.00127	−1.00	0.00178	0.232	0.104	0.254
4.00	−2.0672	0.7003	−0.00125	−1.00	0.00191	0.233	0.100	0.253
5.00	−2.0003	0.6848	−0.00125	−1.00	0.00187	0.235	0.101	0.256
7.50	−1.9082	0.6633	−0.00121	−1.00	0.00180	0.240	0.102	0.261
10.00	−1.8767	0.6600	−0.00118	−1.00	0.00166	0.238	0.114	0.264
15.00	−1.6863	0.6211	−0.00109	−1.00	0.00175	0.236	0.104	0.258

(PGA) less than 1.0 cm/s^2 in one horizontal component are omitted. Events whose focal depths are zero or greater than 200 km are also excluded from the analysis. The final data set consists of 2,166 earthquake records from 387 events recorded in 76 free-field JMA stations (accelerometers are placed on small foundations that are detached from the small housing structure). Table 1 provides a summary of the JMA-87 data set characteristics.

Peak ground motions are also affected by the source mechanism. To convey the information of source mechanism into the predicted peak ground motions, the fault types, i.e., normal and reverse, are included in the attenuation model (Abrahamson and Litehiser 1989; Dicky 1995). Adding this parameter reduces the number of data, because not all earthquakes have information regarding the source mechanism. Moreover, observation of the records shows that some are generated by relatively small earthquakes. The information on fault types from small earthquakes is generally less reliable. Dicky (1995) has used two criteria for data selection from the 2,166 earthquake records from 387 events used in the present study: a magnitude greater than 5 and a horizontal PGA greater than 10 cm/s^2 are required. Using these criteria, 228 three-component records generated by 52 events with known source mechanisms and recorded at 52 JMA stations are obtained. Dicky (1995) has also shown that predicted peak ground accelerations are higher for reverse faults than those for normal faults.

Table 8 (in Appendix I) lists the JMA stations together with station number, station code, latitude, longitude, soil type, and number of records. Generally, JMA recording stations are classified into four soil types according to the presence of soft layers. This classification is commonly used in Japan and is explained in Table 9, also in Appendix I.

The relative spectral velocity, $S_V(\zeta, T)$, used in this study is defined as the maximum response of a ζ (=0, 2, and 5) percent damped single-degree-of-freedom oscillator of varying structural period, T. The responses are calculated by Newmark's direct integration method from the acceleration time histories. The $S_V^H(\zeta, T)$ is computed for both horizontal components, and the larger of the two is used in the regression calculations. The regression is also performed for the vertical velocity response,

TABLE 5. Regression Coefficients for Relative Velocity Response Spectrum $S_V^V(0.02, T)$ (in cm/s)

T (sec) (1)	b_0 (2)	b_1 (3)	b_2 (4)	b_3 (5)	b_4 (6)	σ_r (7)	σ_e (8)	σ (9)
0.05	−2.1394	0.3892	−0.00200	−1.00	0.00490	0.256	0.186	0.317
0.06	−1.9100	0.3966	−0.00211	−1.00	0.00502	0.264	0.191	0.326
0.075	−1.6104	0.4010	−0.00211	−1.00	0.00489	0.261	0.200	0.329
0.10	−1.3084	0.4070	−0.0210	−1.00	0.00487	0.257	0.199	0.325
0.12	−1.1888	0.4162	−0.00203	−1.00	0.00462	0.249	0.187	0.321
0.15	−1.0766	0.4275	−0.00187	−1.00	0.00428	0.246	0.174	0.301
0.17	−1.0868	0.4424	−0.00181	−1.00	0.00411	0.245	0.162	0.307
0.20	−1.0981	0.4584	−0.00171	−1.00	0.00378	0.247	0.148	0.288
0.25	−1.1974	0.4914	−0.00156	−1.00	0.00337	0.235	0.135	0.271
0.30	−1.2719	0.5159	−0.00147	−1.00	0.00304	0.233	0.123	0.264
0.40	−1.5820	0.5819	−0.00139	−1.00	0.00247	0.220	0.128	0.255
0.50	−1.7502	0.6129	−0.00127	−1.00	0.00210	0.209	0.129	0.246
0.75	−2.2143	0.7013	−0.00119	−1.00	0.00142	0.205	0.130	0.243
1.00	−2.4864	0.7458	−0.00100	−1.00	0.00094	0.198	0.125	0.234
1.50	−2.6769	0.7663	−0.00105	−1.00	0.00100	0.191	0.118	0.224
2.00	−2.7361	0.7640	−0.00097	−1.00	0.00107	0.193	0.107	0.221
3.00	−2.7390	0.7549	−0.00109	−1.00	0.00128	0.198	0.112	0.227
4.00	−2.6007	0.7202	−0.00107	−1.00	0.00137	0.196	0.116	0.228
5.00	−2.5317	0.7037	−0.00110	−1.00	0.00149	0.201	0.113	0.231
7.50	−2.3368	0.6609	−0.00096	−1.00	0.00153	0.202	0.117	0.234
10.00	−2.1932	0.6336	−0.00084	−1.00	0.00145	0.202	0.120	0.235
15.00	−1.9450	0.5857	−0.00072	−1.00	0.00150	0.204	0.114	0.234

TABLE 6. Regression Coefficients for Relative Velocity Response Spectrum $S_V^H(0.05, T)$ (in cm/s)

T (sec) (1)	b_0 (2)	b_1 (3)	b_2 (4)	b_3 (5)	b_4 (6)	σ_r (7)	σ_e (8)	σ (9)
0.05	−1.9847	0.3887	−0.00183	−1.00	0.00417	0.270	0.175	0.322
0.06	−1.7199	0.3796	−0.00187	−1.00	0.00434	0.275	0.173	0.325
0.075	−1.4665	0.3844	−0.00195	−1.00	0.00446	0.277	0.184	0.332
0.10	−1.1000	0.3810	−0.00193	−1.00	0.00442	0.277	0.187	0.331
0.12	−0.9171	0.3857	−0.00191	−1.00	0.00432	0.272	0.185	0.329
0.15	−0.7690	0.4010	−0.00181	−1.00	0.00398	0.273	0.177	0.326
0.17	−0.7428	0.4139	−0.00170	−1.00	0.003812	0.273	0.158	0.315
0.20	−0.7260	0.4330	−0.00160	−1.00	0.00348	0.273	0.146	0.310
0.25	−0.8077	0.4702	−0.00153	−1.00	0.00319	0.264	0.142	0.300
0.30	−0.8540	0.4920	−0.00146	−1.00	0.00303	0.261	0.134	0.294
0.40	−1.0390	0.5430	−0.00145	−1.00	0.00267	0.250	0.129	0.282
0.50	−1.1640	0.5700	−0.00138	−1.00	0.00245	0.245	0.115	0.271
0.75	−1.5310	0.6400	−0.00128	−1.00	0.00202	0.240	0.114	0.266
1.00	−1.7950	0.6830	−0.00124	−1.00	0.00183	0.235	0.112	0.260
1.50	−1.9810	0.7050	−0.00124	−1.00	0.00176	0.231	0.104	0.254
2.00	−2.0480	0.7090	−0.00125	−1.00	0.00178	0.231	0.104	0.254
3.00	−2.0580	0.7010	−0.00133	−1.00	0.00198	0.233	0.104	0.255
4.00	−1.9980	0.6840	−0.00130	−1.00	0.00205	0.234	0.101	0.255
5.00	−1.9452	0.6715	−0.00130	−1.00	0.00202	0.236	0.101	0.257
7.50	−1.8932	0.6589	−0.00127	−1.00	0.00193	0.240	0.103	0.261
10.00	−1.8747	0.6574	−0.00123	−1.00	0.00177	0.239	0.111	0.264
15.00	−1.7195	0.6256	−0.00115	−1.00	0.00183	0.239	0.103	0.260

$S_V^V(\zeta, T)$. Twenty-two structural periods from 0.05 to 15 s (Table 1) are selected, and regression analysis is performed separately for each structural period. By treating the attenuation of each structural period as independent from the others, a form of the spectral shape is not imposed. The spectral shape for a given magnitude and distance can be determined by attenuating the expected responses of each structural period to the site.

Fig. 2 shows the distribution of the JMA magnitude, distance, and $S_V(\zeta, T)$ (horizontal and vertical) of the ground motion data used at $T = 0.5$ s and damping equal to 5%.

ATTENUATION MODEL

The attenuation of the response spectrum is assumed to be similar to the attenuation of the peak ground motion parameter as proposed by Molas and Yamazaki (1995a). As with peak ground motion, the attenuation form is taken as the theoretical attenuation of body waves in a continuous medium from a point source with a geometric spreading term, an elastic attenuation term, a depth factor, and a local site factor, and is given by

$$\log y(T) = b_0(T) + b_1(T)M + b_2(T)r + b_3(T)\log r + b_4(T)h + \sum_{i=1}^{N} c_i(T)S_i + \sigma P \quad (1)$$

where $y(T)$ = ground motion index under consideration (in this study, $y(T)$ is either the larger of the two horizontal components or the vertical component); M = JMA magnitude; r = slant distance between the source and the recording station; $b_i(T)$'s = coefficients to be determined and the total variation, σ^2; and $P = 0$ for 50 percentiles and 1 for 84 percentiles. The definition of the JMA magnitude is different for focal depths greater than 60 km. For deep events, the effect of depth and attenuation are taken into consideration, so it is reasonable to use the magnitude scale continuously from shallow to deep events. The term $b_2(T)r$ represents anelastic attenuation; and the term $b_3(T)\log r$ represents geometric spreading. The geo-

TABLE 7. Regression Coefficients for Relative Velocity Response Spectrum $S_V^V(0.05, T)$ (in cm/s)

T (sec) (1)	b_0 (2)	b_1 (3)	b_2 (4)	b_3 (5)	b_4 (6)	σ_r (7)	σ_e (8)	σ (9)
0.05	−2.2472	0.3970	−0.00200	−1.00	0.00480	0.257	0.186	0.317
0.06	−2.0066	0.3967	−0.00210	−1.00	0.00496	0.258	0.193	0.322
0.075	−1.7495	0.4040	−0.00212	−1.00	0.00487	0.259	0.199	0.326
0.10	−1.4370	0.4050	−0.00209	−1.00	0.00479	0.255	0.196	0.322
0.12	−1.3004	0.4115	−0.00203	−1.00	0.00461	0.247	0.186	0.309
0.15	−1.2050	0.4240	−0.00191	−1.00	0.00436	0.246	0.172	0.300
0.17	−1.1929	0.4354	−0.00184	−1.00	0.00416	0.245	0.163	0.294
0.20	−1.2020	0.4520	−0.00175	−1.00	0.00388	0.246	0.148	0.287
0.25	−1.3038	0.4870	−0.00163	−1.00	0.00347	0.236	0.133	0.271
0.30	−1.3690	0.5090	−0.00155	−1.00	0.00321	0.235	0.122	0.265
0.40	−1.6210	0.5660	−0.00145	−1.00	0.00269	0.221	0.126	0.255
0.50	−1.7650	0.5930	−0.00132	−1.00	0.00231	0.212	0.122	0.244
0.75	−2.1890	0.6750	−0.00125	−1.00	0.00175	0.205	0.126	0.241
1.00	−2.4020	0.7120	−0.00109	−1.00	0.00131	0.197	0.121	0.231
1.50	−2.5600	0.7310	−0.00113	−1.00	0.00131	0.194	0.115	0.225
2.00	−2.6300	0.7340	−0.00109	−1.00	0.00141	0.196	0.109	0.225
3.00	−2.6490	0.7310	−0.00117	−1.00	0.00153	0.198	0.113	0.228
4.00	−2.5480	0.7050	−0.00114	−1.00	0.00155	0.198	0.116	0.229
5.00	−2.5012	0.6939	−0.00115	−1.00	0.00165	0.200	0.112	0.230
7.50	−2.3496	0.6610	−0.00106	−1.00	0.00164	0.204	0.116	0.235
10.00	−2.2266	0.6378	−0.00094	−1.00	0.00156	0.203	0.118	0.235
15.00	−1.9908	0.5926	−0.00081	−1.00	0.00158	0.205	0.115	0.235

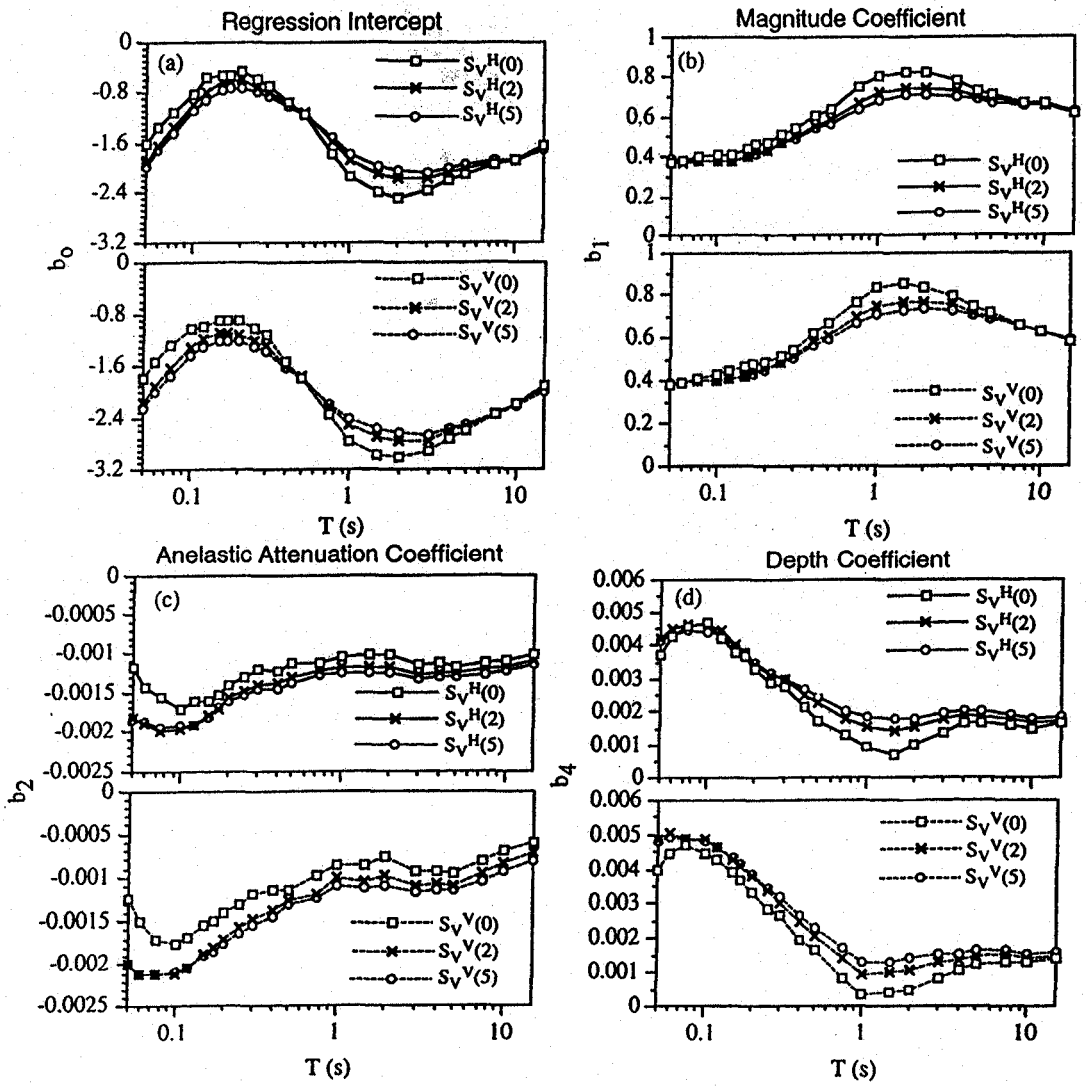

FIG. 3. Regression Coefficients for $S_V^H(\zeta, T)$ and $S_V^V(\zeta, T)$ for Three Damping Ratios (0%, 2%, and 5%): (a) Regression Intercept; (b) Magnitude Coefficient; (c) Anelastic Attenuation Coefficient; (d) Depth Coefficient

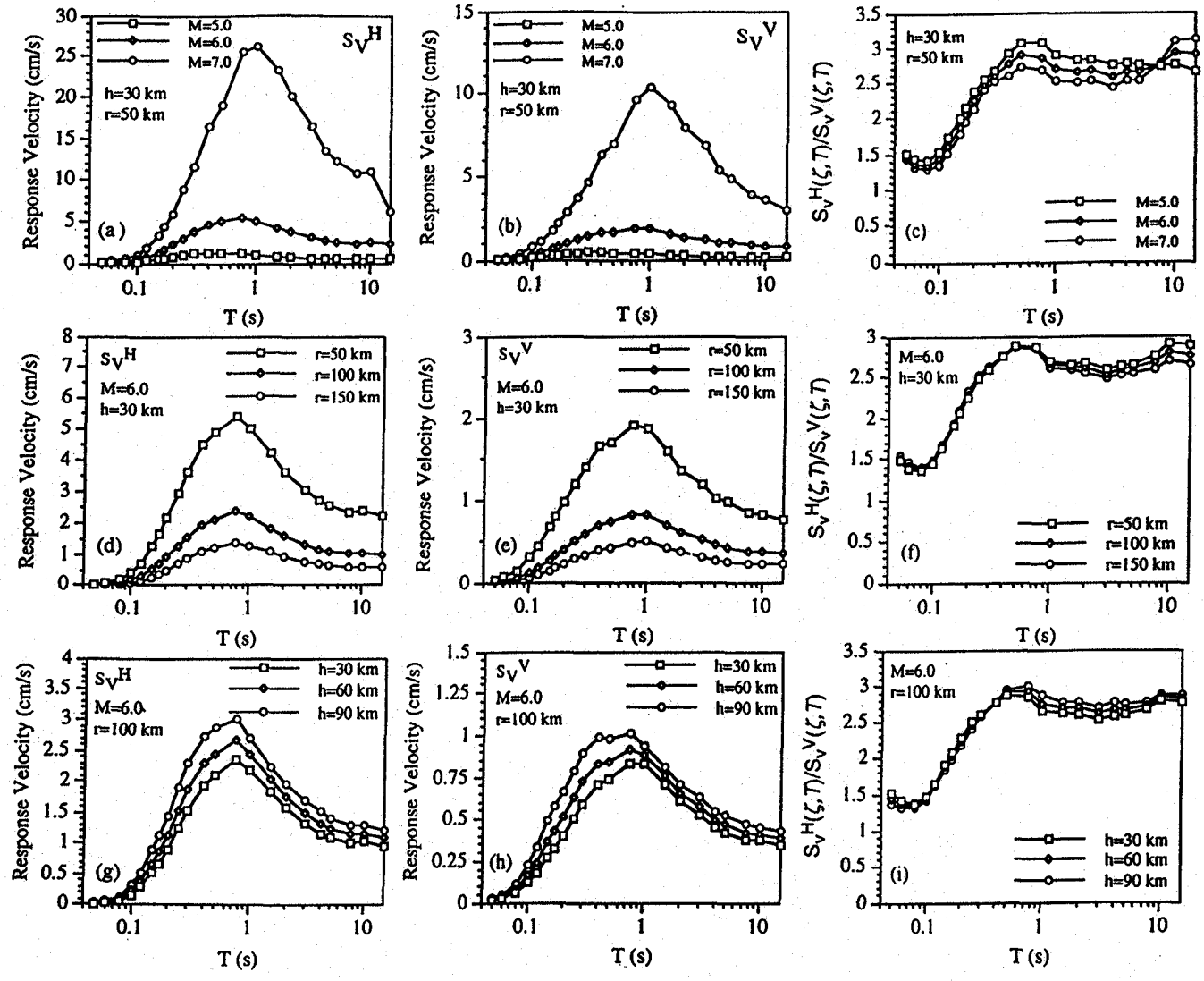

FIG. 4. Predicted Horizontal and Vertical Velocity Spectral Ordinates, and Horizontal-to-Vertical Velocity Response Spectral Ratio at 2% Damping and $c_i = 0.0$

metric spreading term $b_3(T)$ is assumed to be -1. In addition, h = depth in kilometers of the point in the fault plane that is closest to the recording site; $c_i(T)$'s = station coefficients representing the local site effect at the recording site; and $S_i = 1$ for station i and 0 otherwise. It can be added that (1) by itself does not have a unique solution; it is solved by imposing the constraint that the mean of the station coefficient is zero. The total variation, σ^2, is taken as $\sigma^2 = \sigma_r^2 + \sigma_e^2$, where σ_r^2 = the record-to-record component of the variance and σ_e^2 = the earthquake-to-earthquake component of the variance. Though the results are not reported here, preliminary analyses are performed to verify the significance of the depth term and station coefficient to the regression.

Most of the previous studies on the attenuation relation of strong ground motion employ a linear function of magnitude as the source effect, and other prediction models include an M^2 term. In the discussions of Fukushima (1996), the following observations are made: the scaling relation of the spectrum amplitude with M_w (moment magnitude) can be simply approximated by the quadratic model, and the coefficient of the M_w^2 term is negative. On the other hand, the scaling relation of the spectrum amplitude with M (JMA magnitude) may be approximated as a quadratic model for magnitudes greater than 5.5, and the coefficient of the M^2 term is positive. The present study uses the JMA magnitude, and the attenuation relation employs a linear function of magnitude [(1)].

The location of the source is generally assumed to be the center of energy release, which could be estimated by the size of the ruptured fault or by the centroid of the aftershock cluster, if aftershocks are recorded. Here, r is defined as the shortest distance from the recording site to the plane of the fault rupture. However, published reports of fault extent and orientation are difficult to find or even nonexistent for the events in the data set, except for two large earthquakes of magnitude 7.8; namely, the 1993 Kushiro-Oki earthquake (Kagami 1993) and the 1993 Hokkaido-Nansei-Oki earthquake (Nakanishi and Kikuchi 1993). Most of the records are in the far-source, and the third largest event with records close to the fault has a magnitude of 6.6. For the other records, the hypocentral distance is used. As the effect on the regression of the change in distance definition is small in the far-source and for small magnitude events, use of the hypocentral distance is practical and justified.

Because regression analysis is performed for each structural period independently, the index (T) indicating the frequency dependence of each variable has been dropped from the equations, for clarity. It is thus understood that the regression procedure is performed separately for each structural period under consideration.

The attenuation relation of horizontal and vertical components of $S_V(\zeta, T)$ used in this study are as follows:

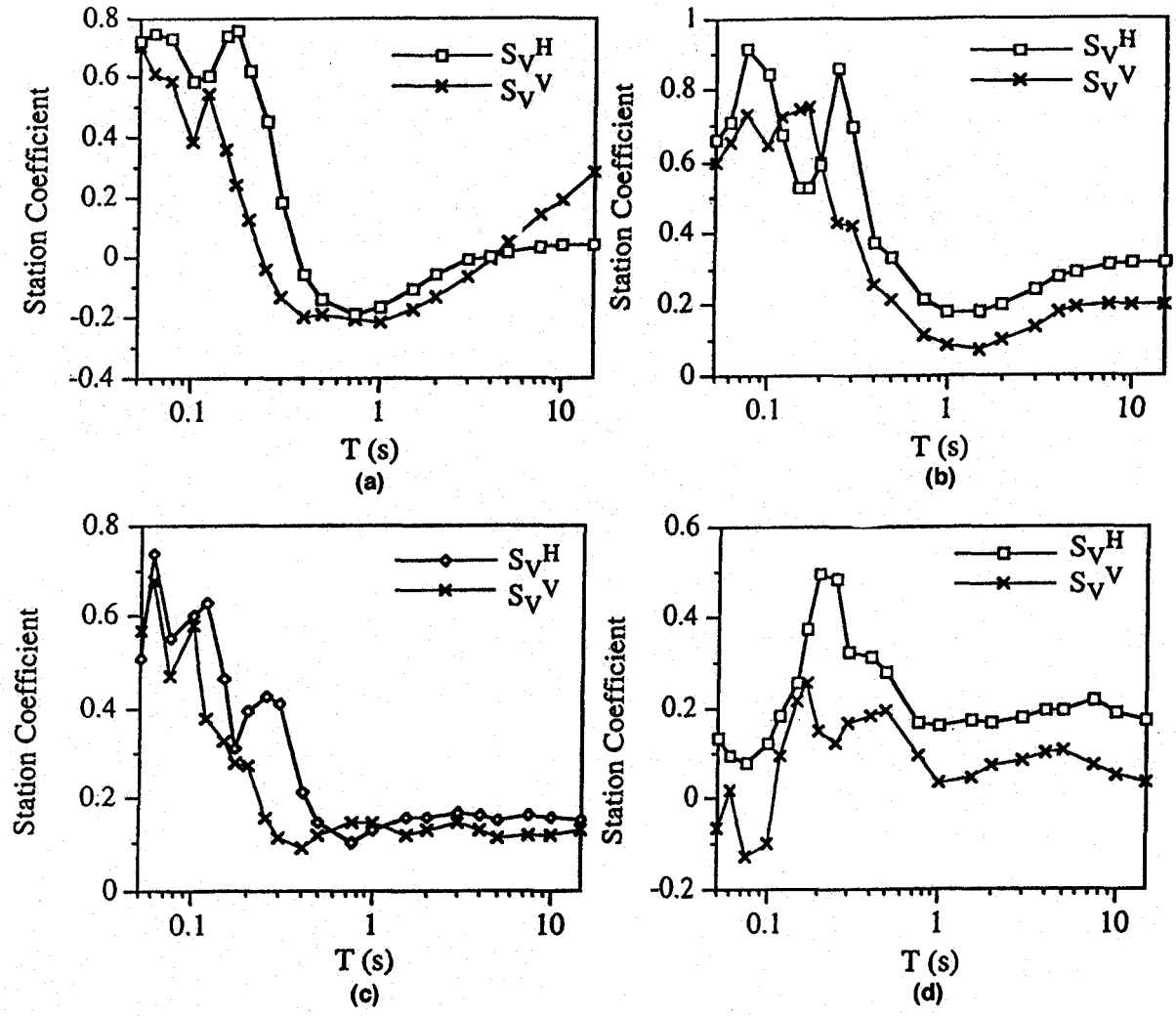

FIG. 5. Comparison of Station Coefficients for $S_V^H(\zeta, T)$ and $S_V^V(\zeta, T)$ for Four JMA Stations at 2% Damping: (a) JMA Hachinohe; (b) JMA Kashiro; (c) JMA Mito; (d) JMA Tokyo

$$\log S_V^H(\zeta, T) = b_0^H + b_1^H M + b_2^H r + b_3^H \log r + b_4^H h + c_i^H + \sigma^H P \quad (2)$$

$$\log S_V^V(\zeta, T) = b_0^V + b_1^V M + b_2^V r + b_3^V \log r + b_4^V h + c_i^V + \sigma^V P \quad (3)$$

Combining (2) and (3), (4) can be obtained as follows:

$$\log \frac{S_V^H(\zeta, T)}{S_V^V(\zeta, T)} = (b_0^H - b_0^V) + (b_1^H - b_1^V)M + (b_2^H - b_2^V)r + (b_4^H - b_4^V)h + (c_i^H - c_i^V) + (\sigma^H - \sigma^V)P \quad (4)$$

METHODOLOGY OF ANALYSIS

In this study, the procedure is applied as described in the following.

The first step determines the coefficients of the regression model given by (1). The second and third steps are similar to the two-stage regression procedure of Joyner and Boore (1981). The second step is the multilinear regression of the equation

$$\log y = \sum_{j=1}^{K} a_j A_j + b_2 r + b_3 \log r + b_4 h + c_i \quad (5)$$

where $A_j = 1$ for earthquake j with magnitude M_j and 0 otherwise; and b_4 and c_i are constrained to the values determined in the previous step. The distance dependence of the attenuation is thus determined. The third step is the regression of the equation

$$a_j = b_0 + b_1 M_j \quad (6)$$

where a_j is determined in the previous step. The third step is carried out with a least squares procedure using the weighting matrix proposed by Joyner and Boore (1993). This step determines the magnitude dependence of the attenuation.

The first step is then repeated, except that b_1 to b_3 are constrained to the values from steps two and three, or

$$\log y = b_0 + b_1 M + b_2 r + b_3 \log r + b_4 h + \sum_{i=1}^{N} c_i S_i \quad (7)$$

where b_1, b_2, and b_3 are constrained. The cycle is repeated until the coefficients stabilize. In this study, ten iterations are used to determine the regression coefficients.

RESULTS AND COMMENTARY

In this study, $S_V^H(\zeta, T)$ and $S_V^V(\zeta, T)$ are estimated from (2) and (3), and $S_V^H(\zeta, T)//S_V^V(\zeta, T)$ is obtained from $S_V^H(\zeta, T)$ and $S_V^V(\zeta, T)$. In the following, regression coefficients, spectra shapes, the spectrum of site coefficients, and the vertical-to-horizontal spectral response ratio are discussed.

Regression Coefficients

The results of the iterative partial regression for the attenuation of horizontal and vertical relative velocity response spectra [$S_V^H(\zeta, T)$ and $S_V^V(\zeta, T)$] are given in Tables 2–7 for

= 0%, 2%, and 5%. Fig. 3 shows a comparison of the structural period dependent regression coefficients for the horizontal and vertical velocity response spectra for the three damping values. In the case of regression intercept b_0, the horizontal component is higher than the vertical component, although the trend is the same for both components. In the very short period range (0.05–0.15 s), b_0 has an increasing trend; in the short period to intermediate period range (0.15–2 s), b_0 has a decreasing trend; and in the long period range (2–15 s), b_0 has a slight increasing trend as the structural period increases.

The magnitude coefficients, b_1, for the horizontal and vertical components are almost the same. The coefficient is nearly constant at periods below 0.1 s; it has an increasing trend as the structural period increases from 0.1–1.5 s; and it has a decreasing trend as the structural period increases from 1.5–15 s. Similar trends have been also observed by Joyner and Boore (1982, 1988).

The anelastic attenuation rate, b_2, becomes more negative as the structural period increases both for horizontal and vertical velocity spectral response. The coefficient for the horizontal component is more negative than that of the vertical component for periods greater than 1 s. In the very short period and longer period ranges, b_2 is almost constant, except when $\zeta = 0\%$. This is consistent with observations that high-frequency contents of strong ground motion are attenuated faster than low-frequency components.

The depth effect term, b_4, decreases as the structural period increases. For the long period range, the horizontal coefficient is greater than vertical one. The depth effect becomes almost constant for periods of 1 s and above. The frequency dependence of the depth effect may be considered a clue as to the physical significance of the depth effect. Molas and Yamazaki (1995a) stated that the depth effect may be caused by the high Q zones travelled by seismic waves from a deep source, resulting in a lower effective attenuation rate and in which case the depth term, b_4, is a kind of adjustment factor. However, the depth effect is also evident for shallow events [Fig. 4(g) and 4(h)]. In this case, the scattering of the seismic waves as it nears the surface results in the effective increase in the attenuation rate. The term hb_4 is larger for deeper events, the sign is opposite that of the anelastic attenuation and geometric spreading terms, and it can consider the depth effect for both shallow and deep events.

In the preceding section, the terms short period and long period structures refer to the response of single-degree-of-freedom systems. Although these uses are made for simplicity, it is important to remember the significance of the two terms.

Because the variation of the attenuation factors due to the three damping ratios is not significant, for the rest of the analysis, $\zeta = 2\%$ has been used.

Spectral Shape

An important aspect of the response spectra is the spectral shape, because this will largely determine the expected response of a given structure. By taking the regression for several structural periods independently, it is not necessary to predetermine the shape of the response spectra. Fig. 4 compares the spectral shapes for different magnitudes, slant distances (r), and source depths (h). It can be seen from this figure that the spectral shape of both the horizontal and vertical velocity responses depends on the magnitude and, to some extent, on distance and depth.

Figs. 4(a) and 4(b) show estimated horizontal and vertical velocity response spectra for a given depth and slant distance with changes in magnitude. Higher responses can be observed for larger magnitudes. The structural period in which the peak of the response curves occurs increases as the magnitude increases. This is consistent with the change of the magnitude term with respect to the structural period [Fig. 3(b)]. Figs. 4(d) and 4(e) show estimated horizontal and vertical velocity response spectra for a given magnitude and depth with changes in the slant distance. Higher responses can be observed for shorter distances. There is a slight shift of the peak to a shorter structural period as the slant distance decreases; this may not be significant for the horizontal component, but it is apparent for the vertical component. Figs. 4(g) and 4(h) show estimated horizontal and vertical velocity response spectra for a given magnitude and slant distance with changes in the depth. Higher responses can be observed for deeper events. It must be noted that these response spectra refer to different sites, because a deeper source with the same slant distance will have a shorter horizontal distance.

Spectral Ratio

Fig. 4 also shows estimated horizontal-to-vertical velocity response spectral ratio for different magnitudes, slant distances (r), and source depths (h). Fig. 4(c) shows the velocity response spectral ratio for a given depth and slant distance with changes in magnitude. In the very short period range (less than 0.1 s), the horizontal-to-vertical ratio is almost constant (about 1.5); in the short period range (0.1–0.5 s), the ratio increases linearly with the period (varying between 1.5 and 3.0); and in the intermediate to long period range (0.5–7.5 s), the ratio is high but constant (about 3.0). In this range of periods, the ratio is high for low magnitude events but for very long period ranges (greater than 7.5 s), the ratio becomes comparatively higher for bigger magnitude events. The high value of the ratio in the short to long period is due to the fact that, predominantly, the low-frequency horizontal component controls the ground motion in this range. A similar trend for far-source records has been observed by Bozorgnia and Niazi (1993).

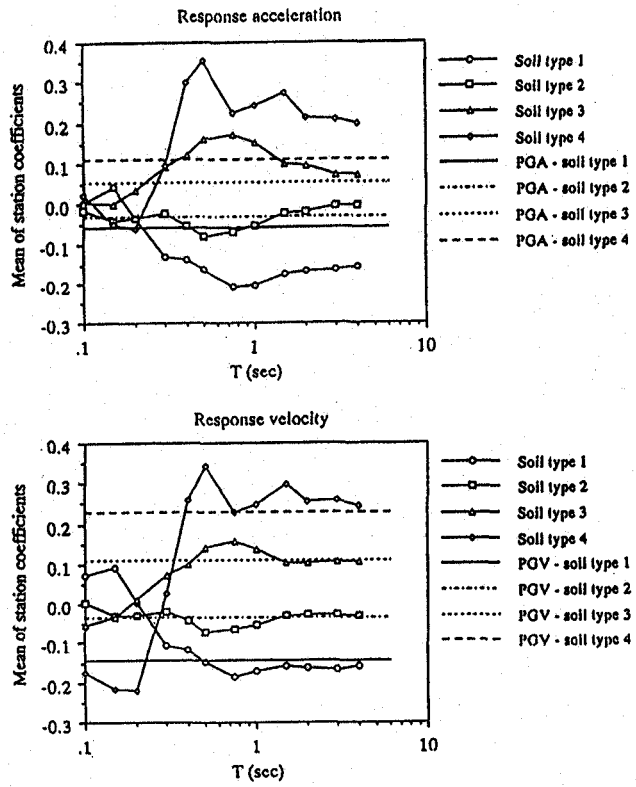

FIG. 6. Spectra of Mean Station Coefficient for Each Soil Type Classification Given in Table 9 of Absolute Horizontal Acceleration (Top) and Relative Horizontal Velocity (Bottom) Response Spectra [Horizontal Lines Show Mean Station Coefficient for Each Soil Type for Peak Ground Acceleration (PGA) and Peak Ground Velocity (PGV)] [From Molas and Yamazaki (1995a)]

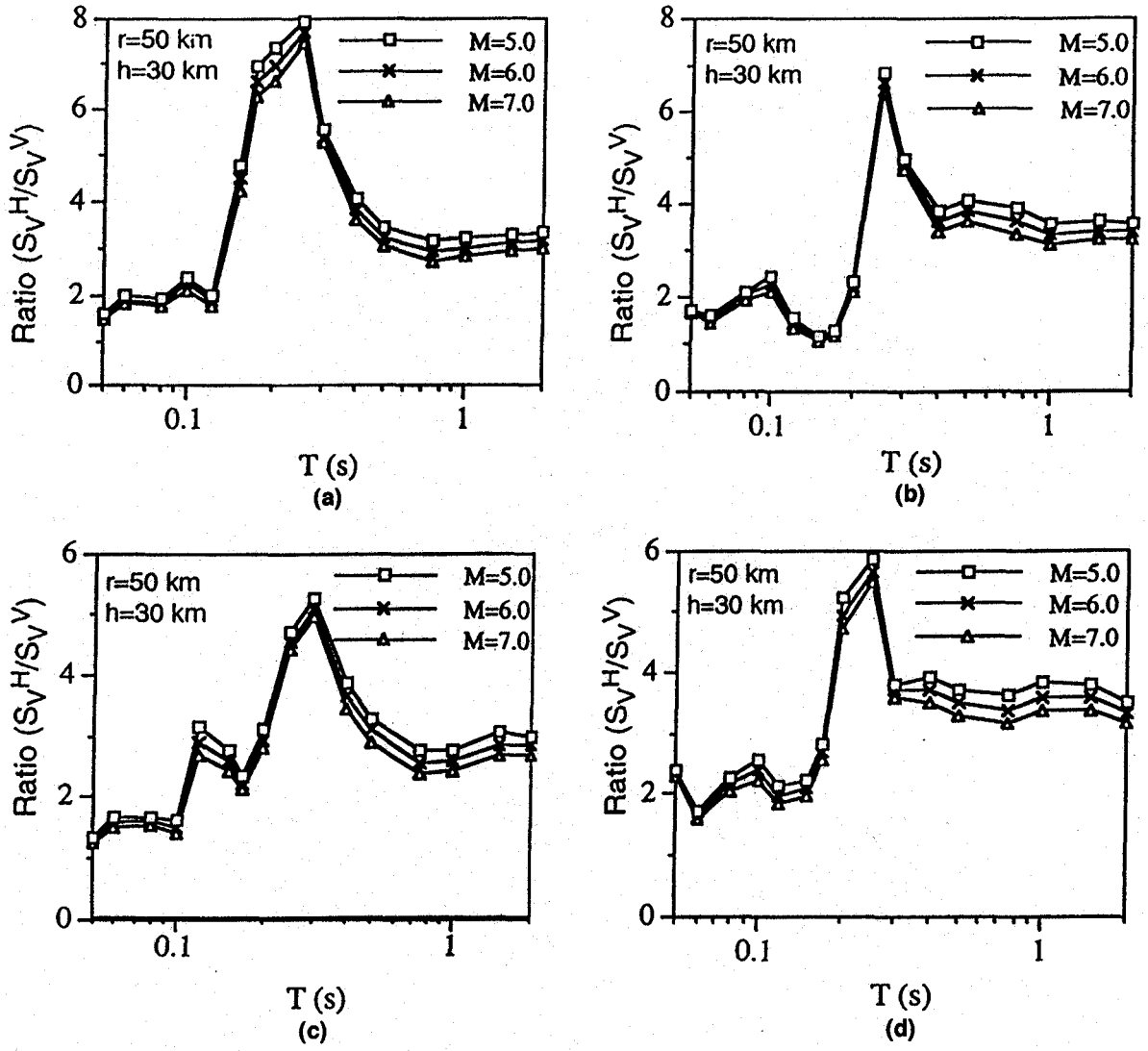

FIG. 7. Predicted Horizontal-to-Vertical Velocity Response Spectral Ratio at 2% Damping for Four JMA Stations: (a) JMA Hachinohe (b) JMA Kushiro (c) JMA Mito; (d) JMA Tokyo

Fig. 4(f) shows the velocity response spectral ratio for a given magnitude and depth with changes in the slant distance. The trend of variation of the ratio with the period is the same as in Fig. 4(c). The effect of the variation of slant distance is negligible. A similar trend may not be true for near-source recordings, where $r < 30$ km. The 1995 Hyogoken-Nanbu Earthquake is the biggest event in Japan that produced some near-source recordings. Molas and Yamazaki (1995b) have shown that near-source data from this event fit the predicted attenuation for far-source JMA-87 data. However, the data is still inadequate for a more definite conclusion. The lack of data prevents this study from showing near-source effects on the horizontal-to-vertical velocity response spectral ratio. However, a substantial body of data from the 1989 Loma Prieta (Bozorgnia and Niazi 1993) and 1994 Northridge earthquake (Bozorgnia et al. 1995) show that distance has a very large effect on the ratio of horizontal-to-vertical response for near-source recordings.

Fig. 4(i) shows the velocity response spectral ratio for a given magnitude and slant distance with changes in the depth. The variation of the ratio with different depths is not significant.

Local Site Effect

The station coefficients determined from the regression can be regarded as the amplification of ground motion of one station relative to the other stations. The regression is performe such that the mean of the station coefficients is zero, as state earlier. Site amplifications are known to be frequency depen dent. The station coefficients of one station for different struc tural periods are therefore not absolutely related to each othe rather, each is related to the mean amplification for eac structural period considered. However, the shape of the spec trum of station coefficients for one station can give useful in formation about the frequency dependence of amplification i the station.

Fig. 5 shows the station coefficient spectrum for S_V^H an S_V^V for four JMA stations. The stations are chosen because o their large number of records (more than 50 records per sta tion), making the determination of station coefficients stable By inspection, the station coefficient spectrum does not sho a dominant trend. The station coefficient spectra are given sep arately for each of the four stations. The figures show tha there is good agreement between the spectra for S_V^H and S_V^V although the shapes are quite different from station to statio Each recording station is classified into four soil types, a given in Table 9 of Appendix I. This suggests that the statio coefficient spectrum may characterize the amplification of site for other ground motion parameters. However, the result in this study are still too small to use as the basis for a mor definite conclusion.

Fig. 6 shows spectra of the mean station coefficient for eac

soil type. The soil types show progressively more amplification at intermediate and long periods as one proceeds from hard to softer sites. At short periods, the sequence is reversed, because the effect of soil damping predominates over amplification, and the softer sites show relative attenuation.

Site-Specific Response Spectral Ratio

Because the local site effect is considered in the regression analysis, the resulting predictive equations for each site are, in effect, site-specific expected response spectra. At first, the expected horizontal and vertical velocity response spectra of the mean station (with $c_i = 0.0$) and the spectrum of station coefficients (c_i^H and c_i^V) are combined to obtain site-specific horizontal and vertical response spectra for each of the JMA recording stations. After that, a site-specific response spectral ratio is obtained by combining horizontal and vertical response spectra for each site. Fig. 7 shows sample site-specific velocity response spectral ratio for the four JMA stations shown in Fig. 5. These spectral ratios are different in terms of the amplitude and shape, and the effect of magnitude on the spectral shape is included. These characteristics are important in the seismic hazard and risk analysis of critical structures.

CONCLUSIONS

In this study, horizontal and vertical relative velocity response spectra at three critical damping ratios are estimated from attenuation relation developed at 22 natural periods using far-source JMA-87 recordings (387 events with 2,166 records at 76 JMA stations). The use of these new records is significant because there is no need to correct for suppressed instrument sensivity in the high-frequency range.

The horizontal and vertical SV values are dependent on magnitude and, to some extent, on distance and depth. It is also observed that the H/V ratio of SV is independent of magnitude, distance, and depth. The H/V ratio of SV at a very low period range shows a value similar to the standard 1.5, but at a low to intermediate period range, the H/V ratio of SV varies between 1.5 to 3.0. At a long period range, it stabilizes to 3.0.

The frequency dependence of the station coefficients is found to be specific to a recording station. There is apparent correlation to the soil type classification of the recording site, and the mean of the station coefficients for each soil type follows the general trend that larger ground motion is expected as the ground becomes softer.

By introducing station coefficients and representing site amplification to the horizontal-to-vertical ratios of the velocity response spectra, site-specific spectral ratio can be obtained.

APPENDIX I.

TABLE 8. List of Japan Meteorological Agency (JMA) Stations

Station number (1)	Station code (2)	Station name (3)	Latitude (N) (4)	Longitude (E) (5)	Soil type (6)	Number of records (7)
1	ABJ	Abashiri	44.015	144.283	2	14
2	AJI	Ajiro	35.043	139.097	2	80
3	AKI	Akita	39.715	140.103	3	17
4	AOM	Aomori	40.820	140.773	4[a]	56
5	ASA	Asahikawa	43.770	142.373	2	7
6	ASZ	Ashizuri	32.720	133.013	1	3
7	CHO	Choshi	35.737	140.862	2[a]	48
8	FKK	Fukuoka	33.580	130.380	2	6
9	FUK	Fukui	36.053	136.227	4	16
10	FUN	Kawaguchiko	35.498	138.763	1	36
11	HAC	Hachinohe	40.525	141.525	2	107
12	HAK	Hakodate	41.815	140.758	3	38
13	HIK	Hikone	35.273	136.247	3	15
14	HIR	Hiroshima	34.395	132.465	2[a]	12
15	HJJ	Hachijojima	33.102	139.788	2[a]	40
16	HMD	Hamada	34.893	132.073	1	5
17	HMM	Hamamatsu	34.707	137.723	2	16
18	IID	IIDA	35.510	137.837	2	20
19	ISI	Ishigakijima	24.332	124.163	1	8
20	ISN	Ishinomaki	38.425	141.303	2	48
21	KAG	Kagoshima	31.573	130.553	2	9
22	KAN	Kanazawa	36.587	136.637	3	10
23	KOB	Kobe	34.688	135.180	2	4
24	KOF	Kofu	35.665	138.557	3	48
25	KTR	Katsuura	35.148	140.315	3[a]	28
26	KUM	Kumamoto	32.810	130.710	2	7
27	KUS	Kushiro	42.975	144.392	3	56
28	MAE	Maebashi	36.402	139.065	2	31
29	MAT	Matsushiro	36.547	138.213	1	2
30	MIS	Mishima	35.112	138.930	2	39
31	MIT	Mito	36.378	140.472	2	100
32	MRK	Morioka	39.697	141.167	2	103
33	MRT	Murotomisaki	33.248	134.180	1	4
34	MTM	Matsumoto	36.243	137.973	2	10
35	MTS	Matsue	35.455	133.072	1	7
36	MTY	Matsuyama	33.840	132.780	2	7
37	MYK	Miyakojima	24.792	125.278	1	3
38	MYZ	Miyazaki	31.920	131.423	3	13
39	MZH	Maizuru	35.448	135.320	3[a]	6
40	NAG	Nagoya	35.165	136.968	2	19
41	NAH	Naha	26.203	127.690	1	6
42	NEM	Nemuro	43.328	145.590	1	40
43	NGT	Irozaki	34.600	138.847	1	23
44	NII	Niigata	37.910	139.052	3	12
45	NOB	Nobeoka	32.578	131.660	1	5
46	NZJ	Naze	28.377	129.498	3[a]	12
47	OFU	Ofunato	39.062	141.718	1	79
48	OIT	Oita	33.233	131.623	3	10
49	OKA	Okayama	34.658	133.918	2	13
50	OMA	Omaezaki	34.603	138.213	2	16
51	ONA	Onahama	36.945	140.907	3	79
52	OSA	Osaka	34.678	135.522	3	5
53	OSH	Oshima	34.747	139.367	1	58
54	SAK	Sakata	38.907	139.847	4	19
55	SAP	Sapporo	43.058	141.332	2	15
56	SEN	Sendai	38.260	140.900	2[a]	66
57	SHJ	Shionomisaki	33.448	135.763	2	4
58	SHN	Shimonoseki	33.945	130.928	4	6
59	SHZ	Shizuoka	34.973	138.407	3	32
60	SUT	Suttsu	42.793	140.228	2[a]	7
61	TAJ	Tanegashima	30.737	130.993	1	6
62	TAT	Tateyama	34.983	139.868	3	65
63	TKD	Takada	37.105	138.250	3	13
64	TKY	Takayama	36.153	137.257	2	10
65	TMR	Tomakomai	42.623	141.585	3	56
66	TOK	Tokyo	35.687	139.758	3	99
67	TOT	Tottori	35.485	134.240	3	7
68	TOY	Toyama	36.707	137.205	2	13
69	TSU	Tsu	34.730	136.523	3	12
70	URA	Urakawa	42.158	142.782	1	84
71	UTS	Utsunomiya	36.547	139.872	2	65
72	WAJ	Wajima	37.390	136.898	3	17
73	WAK	Wakkanai	45.413	141.683	2	2
74	WKM	Wakamatsu	37.485	139.913	2[a]	27
75	YOK	Yokohama	35.437	139.657	2	82
76	YON	Yonago	35.432	133.342	3	3

Note: JMA stations in Izuhara and Uwajima are not included because they do not have records used in this study.
[a]Unconfirmed soil type classification.

TABLE 9. Classification of Ground Conditions for JMA Stations

Soil condition (1)	Geological definition (2)	Definition by natural period (3)
Type 1 (rock)	Tertiary or older rock (defined as bedrock) or diluvium with $H < 10$ m	$T < 0.2$ s
Type 2 (hard soil)	Diluvium with $H \geq 10$ m, or alluvium with $H < 10$ m	$0.2 \leq T < 0.4$ s
Type 3 (medium soil)	Alluvium with $H < 25$ m, including soft layer with thickness less than 5 m	$0.4 \leq T < 0.6$ s
Type 4 (soft soil)	Other than above, usually soft alluvium or reclaimed land	$T \geq 0.6$ s

APPENDIX II. REFERENCES

Abrahamson, N. A., and Litehiser, J. J. (1989). "Attenuation of vertical peak acceleration." *Bull. Seismological Soc. of Am.*, 79, 549–580.

Bozorgnia, Y., and Niazi, M. (1993). "Distance scaling of vertical and horizontal response spectra of the Loma Prieta Earthquake." *Earthquake Engrg. and Struct. Dynam.*, 22, 695–707.

Bozorgnia, Y., Niazi, M., and Campbell, K. W. (1995). "Characteristics of free-field vertical ground motion during the Northridge Earthquake." *Earthquake Spectra*, 11, 515–525.

Dicky, L. (1995). "Analysis of vertical ground motion characteristics by using JMA-87 accelerometer data," M. Eng. thesis, Dept. of Civil Engineering, University of Tokyo, Tokyo, Japan.

Fukushima, Y. (1996). "Scaling relations for strong ground motion prediction models with M^2 terms." *Bull. Seismological Soc. of Am.*, 86, 329–336.

Joyner, W. B., and Boore, D. M. (1981). "Peak horizontal acceleration and velocity from strong motion records including records from 1979 Imperial Valley, California, earthquake." *Bull. Seismological Soc. of Am.*, 71, 2011–2038.

Joyner, W. B., and Boore, D. M. (1982). "Estimation of response spectral values as functions of magnitude, distance and site conditions." *Open File Rep. 82-881*, U.S. Geological Survey, Denver, Colo.

Joyner, W. B., and Boore, D. M. (1988). "Measurement, characterization and prediction of strong ground motion." *Proc., Earthquake Engrg. and Soil Dynam.*, ASCE, Reston, Va., 43–102.

Joyner, W. B., and Boore, D. M. (1993). "Methods for regression analysis of strong-motion data." *Bull. Seismological Soc. of Am.*, 83, 469–487.

Kagami, H. (1993). "Damage survey of the 1993 Kushiro-Oki earth quake." *Rep. of Japan Ministry of Education, Science, and Cultur Grant No. 04306025*, Japan Ministry of Education, Science, and Culture, Tokyo, Japan, 19–25 (in Japanese).

Lee, V. W. (1993). "Scaling PSV from earthquake magnitude, local soil and geologic depth of sediments." *J. Geotech. Engrg.*, ASCE, 119(1) 108–126.

Mamula, L., Kudo, K., and Shima, E. (1984). "Distribution of ground motion amplification factors as a function of period (3–15 sec), ir Japan." *Bull. Earthquake Research Institute*, 59, 467–500.

Molas, G. L., and Yamazaki, F. (1995a). "Attenuation of earthquak ground motion in Japan including deep focus events." *Bull. Seismological Soc. of Am.*, 85, 1343–1358.

Molas, G. L., and Yamazaki, F. (1995b). "Attenuation of ground motior during the 1995 Great Hanshin Earthquake." *Bull. Earthquake Resistant Structure Research Center*, 28, 25–41.

Nakanishi, I., and Kikuchi, M. (1993). "Characteristics of the 1993 Hokkaido-Nansei-Oki earthquake." *J. Japan Soc. for Earthquake Engrg. Promotion (NEWS)*, 133, 1–5 (in Japanese).

Ohsaki, Y. (1994). *Introduction to spectral analysis of earthquake ground motion*. Kajima Publishing Company, Tokyo, Japan (in Japanese).

Trifunac, M. D., and Lee, V. W. (1989). "Empirical models for scaling Fourier amplitude spectra of strong ground acceleration in terms of earthquake magnitude source to station distance, site intensity and recording site conditions." *Soil Dynam. and Earthquake Engrg.*, 8, 110–125.